Modelling of cyclic visco-elasto-plastic one dimensional behaviour of polyamide-based woven strap

A Blaise, Guilhem Bles, W Dib, M Shash, A Tourabi

Modelling of cyclic visco-elasto-plastic one-dimensional behaviour of polyamide-based woven strap

A. Blaise [a,1], G. Bles [b,2], W. Dib [c], M. Shash [d], A. Tourabi [a,1]

[a] Grenoble-INP, Université Grenoble Alpes, CNRS UMR 5521, 3SR Lab, Grenoble F-38041, France

[b] ENSTA Bretagne, Institut de Recherche Dupuy de Lôme, IRDL-UMR CNRS 6027, 29200, Brest, France

[c] Faculty of Technical Engineering, University of Tartous, Tartous, Syria

[d] Damascus University, Faculty of Mechanical & Electrical Engineering, Department of Mechanical Design Engineering, Damascus, Syria

[1] www.3sr-grenoble.fr

[2] www.irdl.fr

Abstract

This study focuses on modelling of mechanical behaviour of threadlike woven materials or shaped in uniaxial form such as wires, ropes, woven lines, cables, straps, slings etc. The proposed one-dimensional model is based on the superimposition of two stress contributions: a non-Newtonian visco-elastic stress and a time-independent stress. The time-independent stress stands for a particular irreversible behaviour, linked to the loading history. This model neglects the thickness of the time independent hysteresis loops during the unloading-reloading processes while preserving the irreversible character of elastoplastic type behaviour. The model's predictions are compared to a set of experimental results, carried out on polyamide 6-6 (PA66) straps. The model describes the shape of the stress-strain hysteresis loops very well and predicts perfectly the direction of the strain or stress evolution during the creep or relaxation periods, regardless of their position in the first load or in the load-unload branches.

I) Introduction

Although the use of textile materials is ancient, nowadays they could be still unique efficient solutions to current engineering challenges, because of the great mechanical properties of innovative synthetic fibres. Thus, the class of threadlike woven materials or shaped in uniaxial form (wires, ropes, woven lines, cables, straps, slings etc.) is of growing interest in many areas of industry and everyday life. We can mention some of these interesting applications: 1- Firefighters use textile polyamide ropes in case of emergency escape from buildings on fire; [1] as well as, in construction and roofing industries, work-related falls are mitigated by using synthetic fabric; [2] another application in this area is related to sport climbing activity and uses widely textile polymer ropes, notably polyamide ropes for absorbing the fall energy. 2- In the offshore oil and gas industry, for the heavy-load lifting on board of an installation vessel, steel wires are replaced by textile synthetic ropes; this reduces the injury risk for the workers, mainly due to their lightness; in the same way, the mooring of floating offshore platforms used usually steel-chain and steel-wire mooring lines, but, since the 90's, mooring lines made of textile polyester synthetic ropes were designed and used with success for deepwater moorings, where the own weight of the steel lines becomes too high; [3-6] more recently, a new mooring rope is studied as candidate for the floating offshore wind turbine, which corresponds to a laid-strand polyamide synthetic rope. [7,8] 3- The French space agency (CNES) proposes stratospheric balloons, that can carry scientific measurement devices up to altitudes of 40 km. Its main structural part is made of polymer-fibre woven straps, that link the balloon with the scientific devices and others necessary to pilot the flight; as well as, textile synthetic woven straps are also used as structural mechanical link within parachute systems, due to their good strength-to-weight ratio and also to their ability to absorb shocks. [9] 4- New pulley concepts is recently proposed, where the ball bearing is

replaced by an UHMWPE-fibre (e.g. Dyneema, Spectra) braided loop; this reduces the weight and increases the robustness of the system. [10,11] 5- Some tires need fibre reinforcement; nylon, polyester or aramid cords are used. [12-16] 6- Manipulator or robot arms are designed, such that the transmission of the actuator loads to the parts of the arm are performed by aramid yarns [17] ; Kevlar fibre, like Dyneema, Spectra or Vectran, has a great stiffness-to-weight ratio, and could be very useful for this type of application by minimizing the final weight of the product.

In most applications of threadlike woven materials, the tensile mechanical behaviour has to be precisely understood. For example, the mooring lines of floating platform encounter cyclic and also creep tensile loadings. The permanent elongation of these ropes, due to cyclic loading or creep, has a negative impact on the platform movements because of a relaxation of the mooring tension loads. In other applications, where the material is used as a fall energy absorber, the viscous behaviour has to be precisely known for limiting the mechanical acceleration undergone by the workers, parachutists or parachuted devices.

For this reason, a lot of authors worked towards the modelling of the cyclic visco-elasto-plastic behaviour of textile polymer-fibre ropes. The elastic behaviour of laid-strand synthetic ropes has been predicted by analytical models. [18-22] Experimental studies on synthetic ropes for deep water mooring were performed and properties have been studied such as: axial stiffness, hysteresis, creep, recovery, relaxation as a function of the mean load and load range. [3-5, 23-26] The authors Bles [27] ; Bles et al. [9] ; Dib et al. [28] proposed one-dimensional visco-elasto-plastic constitutive laws for woven straps and synthetic fibres based on the superimposition of stress contributions of different natures. The model of Bles, Nowacki and Tourabi [9] was adopted and adapted with success to aramid yarns by Che et al. [17], for modelling the cyclic

mechanical behaviour of robot arms. The authors [29-32] proposed constitutive laws for aramid and polyester yarns and ropes based on two summed strain contributions: viscoplastic and viscoelastic (Schapery's model). Other authors have proposed a behaviour model pattern for polyester mooring ropes of which the strain is a function of the mean and the maximum tensions. [6,33-35] Some authors limited their model to elasto-plastic or to damaged elasticity behaviour of nylon tire cord, despite the strong viscosity of the material. [15] Based on the Flory's pattern, Chevillotte et al. [8] proposed a visco-elasto-plastic law for polyamide laid-strand mooring ropes. This model is based on a non-linear dynamic elasticity, a delayed elasticity, the moduli of which are linear functions of the tensile stress.

Bles et al. [9] carried out cyclic tests on PA66 straps and revealed their visco-elastoplastic behaviour under cyclic loading, using a visco-elasto-hysteresis 1D model. This model is based on the superimposition of three stress contributions, respectively: non-Newtonian viscoelastic, nonlinear elastic and time independent hysteresis. In 2018, Dib et al. [28] have proposed a 2D model to take into account the visco-elastoplastic behaviour of woven materials constituted by 1D fibres arranged in warp and weft, as well as a protection coating. The model used by the authors to describe the visco-elastoplastic behaviour of the fibres is a simplification of the 1D model of Bles et al. [9] Indeed, on one hand, this model neglects the thickness of the time independent hysteresis loops during the unloading-reloading processes while preserving the irreversible character of elastoplastic type behaviour. On the other hand, the non-Newtonian viscous part of the behaviour has a simpler definition, independent of the fibre deformation. The objective of the present work is to propose a simplified visco-elastoplastic 1D model, inspired of the Dib et al. [28] model and to compare its predictions with the experimental results obtained by Bles et al. [9] in order to appraise its validity and the relevance of its assumptions.

II) Experimental aspects

In the present paper, we get inspired of previous works where experimental aspects were fully described in Bles et al. [9] This paragraph reminds the context and is a summary of the mentioned paper where more details can be found. It concerns experimental study of straps samples manufactured by weaving polyamide 6-6 (PA66) strands, a semi-crystalline polymer. Three groups of straps were tested and were called A, B and C. The tests are identified with a three-character code such as Axy, Bxy or Cxy, where A, B and C correspond to the strap groups and the both last characters xy correspond to the test serial number. In this paper, we put forward results from tests performed mainly on the group A. A full description of the geometric parameters of the straps and also of the experimental device can be found in Bles et al. [9] We consider that the straps material studied in the present paper can be seen as a homogeneous continuum and it can be likened to a particular one-dimensional behaviour (1D) whose rigidity in compression is negligible. Thus, according to the assumptions of continuum mechanics, we put forward the Cauchy stress σ defined as: $\sigma = F/S$ where F is the applied load and S is the cross-section of the strap. The experimental device is equipped with an extensometer in order to get a measure of local strain ε in the central part of sample, such as $\varepsilon = (b - b_0)/b_0$, where b and b_0 are respectively the current length and the initial length measured by the extensometer.

III) Constitutive Model

1) Modelling hypotheses

Previous works (Dib et al. [28]) put forward a 2D model in order to describe heterogeneous material behaviour such as complex woven materials, with different fibres orientations and a coating; in the aim of predicting the mechanical behaviour of coated woven fabric and

application to finite element analysis of structures such as complete boat sails. It could take into account the individual behaviour of the warp yarns, the weft yarns, the coating and also their interaction, depending on the yarns orientation, by focusing on the non-Newtonian viscous behaviour, the time-independent irreversibility, the anisotropy and the cyclic loading behaviour. This model was presented in using the notion of specific stress in order to overcome the difficulty of the cross-section measurement of a woven material. In the present paper, we intend to introduce a 1D visco-elastoplastic model inspired by the 1D model proposed by the authors to describe the behaviour of the fibres and in order to model the 1D experimental results obtained by Bles et al. [9] This model corresponds to a simplification of the model proposed by Bles et al. [9], to analyse their experimental results. Indeed, the hysteresis loops linked to the time independent irreversibility during the unloading/reloading processes are neglected. This leads to an elastoplastic type model which keeps its time independent irreversible character with the addition of a reversible behaviour assumption during the unloading/reloading processes. In addition, we consider here, a second simplification compared to the model of Bles et al. [9] which concerns the viscous part of the behaviour. This part will be modelled by a contribution of non-Newtonian visco-elastic stress, independent of the strain. Finally, the model keeps a non-Newtonian viscous character with an irreversible time-independent contribution. Taking into account the assumption of homogeneity of the material of the strap and the choice used to express of the experimental results in Bles et al. [9], the simplified model proposed within this framework will be expressed using the Cauchy stress.

2) Main properties of the one-dimensional constitutive model

In the proposal, the straps mechanical behaviour is described by a one-dimensional model inspired of the works of Dib et al. [28] To analyse the experimental data and characterize the complex cyclic behaviour of the straps, Bles et al. [9] adopted a visco-elasto-hysteresis model. This relatively complex model enables the analysis of the behaviour of the strap material, without requiring phenomenological simplifications compared to experimental observations. Thus, all the characteristics of the behaviour observed experimentally can be taken into account by this model.

Figure 1 summaries the rheological model of Bles et al. [9] It put forward the assumption of stress superimposition, corresponding to different physical phenomena that occur when the straps undergo mechanical actions. The total stress $\sigma(\varepsilon, \dot{\varepsilon}, \xi)$ appears as the sum of two terms: (i) $\sigma_{\underline{v}}(\varepsilon, \dot{\varepsilon})$ a non-Newtonian visco-elastic stress contribution, described by a Maxwell-like model depending on strain ε and strain rate $\dot{\varepsilon}$ and (ii) $\sigma_{\underline{ti}}(\varepsilon, \xi) = \sigma_{r}(\varepsilon) + \sigma_{h}(\varepsilon, \xi)$, a time-independent elasto-hysteresis stress contribution, constituted by the superimposition of $\sigma_{\underline{r}}(\varepsilon)$, a reversible stress contribution of non-linear elastic type and $\sigma_{\underline{h}}(\varepsilon, \xi)$ an hysteresis stress contribution, with an elastoplastic character, depending on reference states indexed by a parameter ξ.

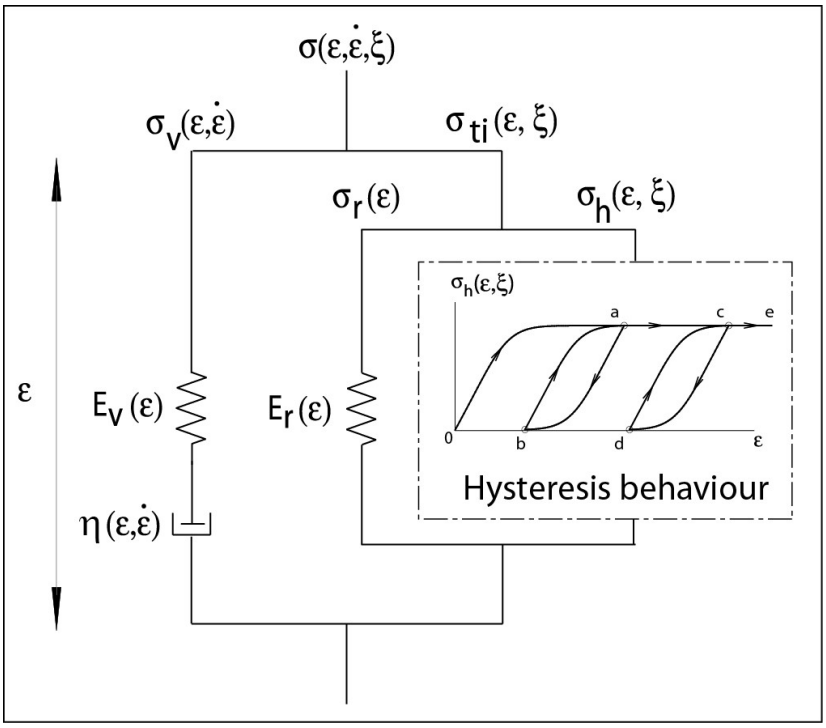

Figure 1: Summary of the rheological model adopted in Bles et al. [9]

We intent to resume the Bles et al. [9] model and perform major simplifications that lie in two considerations; on the one hand, for the viscous stress part, the elastic modulus $E_v(\varepsilon)$ and the viscosity $\eta(\varepsilon, \dot{\varepsilon})$ will be considered as independent of strain ε; consequently, $E_v(\varepsilon)$ remains constant and will be denoted K and $\eta(\varepsilon, \dot{\varepsilon})$ that depends only on $\dot{\varepsilon}$ will be denoted $\eta(\dot{\varepsilon})$ (Figure 2); on the other hand, for the time independent stress part, the hysteresis loop during unloading/reloading process is neglected and replaced by a reversible unloading/reloading hypothesis; then during this process, the behaviour is described by a non-linear elastic behaviour. Indeed, $\sigma_r(\varepsilon)$ and $\sigma_h(\varepsilon, \xi)$ branches merge to only one branch $\sigma_{ti}(\varepsilon)$, assigned to a non-linear elastic behaviour. It means that the branches a-b-a and c-d-c of the Figure 1 are replaced by the branches a-b-a and c-d-c displayed on Figure 2. Figure 2 summarizes this new model that can be considered as a Zener-like rheological model defined by two stress contributions corresponding to: (i) $\sigma_v(\dot{\varepsilon})$, a non-Newtonian visco-elastic stress and (ii) $\sigma_{ti}(\varepsilon)$,

a time-independent stress, that stands for a particular irreversible behaviour, linked to the loading history, which presents an irreversible non-linear behaviour during first loading (branch 0-a-c-e in Figure 2) and a non-linear elastic behaviour during unloading-reloading processes (branches a-b-a and c-d-c in Figure 2). Then, the total Cauchy stress $\sigma(\varepsilon, \dot{\varepsilon})$ in the strap can be expressed by:

$$\sigma(\varepsilon, \dot{\varepsilon}) = \sigma_v(\dot{\varepsilon}) + \sigma_{ti}(\varepsilon) \qquad (1)$$

The detailed structure of the model for $\sigma_{ti}(\varepsilon)$ will be provided in the next section. This section will give the complete definition of the Zener-like rheological model, used to describe the behaviour of the straps.

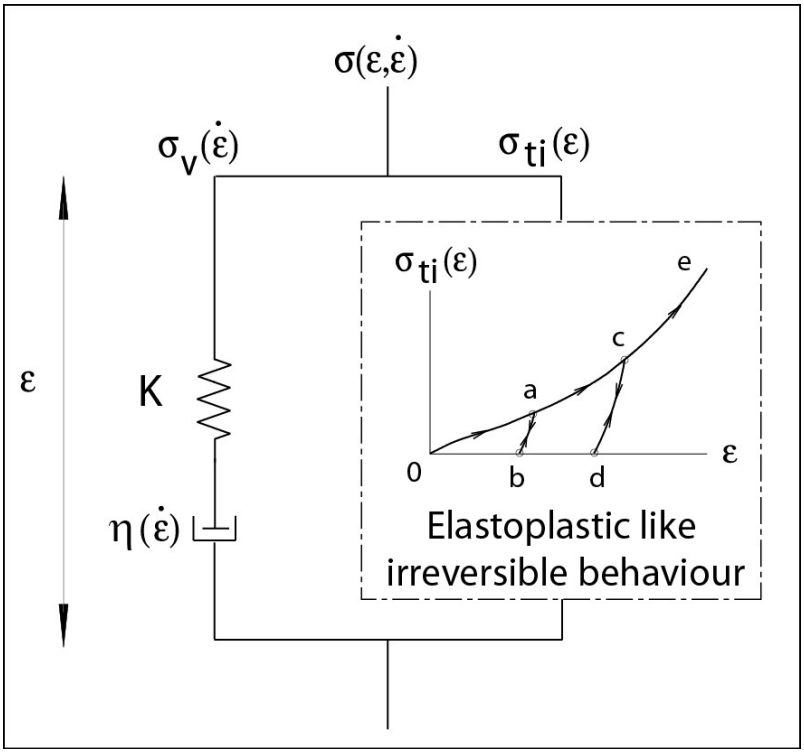

Figure 2: Zener-like one-dimensional model adopted for the description of the mechanical behaviour of the straps. The total stress $\sigma(\varepsilon, \dot{\varepsilon})$ is composed of a non-Newtonian visco-elastic contribution $\sigma_v(\dot{\varepsilon})$ and an irreversible time-independent stress $\sigma_{ti}(\varepsilon)$.

3) Definition of the stress contributions of the model

In this paragraph, we propose to precisely define the contributions $\sigma_{ti}(\varepsilon)$ and $\sigma_v(\dot{\varepsilon})$ which are involved in the Zener-like rheological model adopted in the context of this paper. This model is inspired by the one-dimensional model proposed by Dib et al. [28] to describe the behaviour of the fibres.

a) Irreversible time-independent contribution

According to Dib et al. [28], the irreversible time independent behaviour is defined with the sum of two non-linear elastic-type laws $\mathcal{L}_1(\varepsilon^R)$ and $\mathcal{L}_2(\Delta\varepsilon)$; where $\mathcal{L}_1(\varepsilon^R)$ stands for the stress state during first load and is a function of a reference strain ε^R, that is equal to the model strain ε in the case of monotonic loading; $\mathcal{L}_2(\Delta\varepsilon)$ describes the stress state part during a cycle (unloading/reloading steps) and depends on the variation $\Delta\varepsilon$ between the reference strain ε^R and the actual strain ε such as $\Delta\varepsilon = \varepsilon - \varepsilon^R$; the reference strain ε^R represents the memorised strain at load-inversion point during a first load. This means that ε^R remains constant during the unloading/reloading sequences and its value can only increase, with deformation ($\varepsilon^R = \varepsilon$), when returning to first loading curve. In fact, ε^R is the maximum of actual strain ε along its time evolution. Thus, we define the irreversible time independent stress $\sigma_{ti}(\varepsilon)$ such as:

$$\sigma_{ti}(\varepsilon) = \mathcal{L}_1(\varepsilon^R) + \mathcal{L}_2(\Delta\varepsilon) \qquad (2)$$

During the first load, as the reference strain corresponds to the actual strain ($\varepsilon^R = \varepsilon$) the variation $\Delta\varepsilon$ is null ($\Delta\varepsilon = 0$) which implies that $\mathcal{L}_2(\Delta\varepsilon) = 0$ and that the irreversible time-independent stress becomes:

$$\sigma_{ti}(\varepsilon) = \mathcal{L}_1(\varepsilon^R) \quad \text{and} \quad \varepsilon^R = \varepsilon \qquad (3)$$

Dib et al. [28] proposed a general formulation of $\mathcal{L}_1(\varepsilon^R)$ (in their Eq. 32), which can be adapted to different kind of behaviours:

$$\mathcal{L}_1(\varepsilon^R) = (G - L).\varepsilon^*.\tanh\left(\frac{\varepsilon^R}{\varepsilon^*}\right) + L.\varepsilon^R + H.(\varepsilon^R)^2 + N.(\varepsilon^R)^3 \qquad (4)$$

Where G, L, H,N and ε^* are five material constants. In the present case, we consider a simpler modelling where $G = L$ and $N = 0$. Thus, the irreversible time-independent stress, during the first loading, depends only on two parameters G and H such as (Figure 3):

$$\mathcal{L}_1(\varepsilon^R) = G.\varepsilon^R + H.(\varepsilon^R)^2 \quad \text{and} \quad \varepsilon^R = \varepsilon \qquad (5)$$

During cyclic sequences, ε^R is constant and corresponds to the strain at inversion point on the first load. Consequently, $\mathcal{L}_1(\varepsilon^R)$ remains constant whereas $\mathcal{L}_2(\Delta\varepsilon)$ becomes different from zero, thus:

$$\sigma_{\text{ti}}(\varepsilon) = \mathcal{L}_1(\varepsilon^R) + \mathcal{L}_2(\Delta\varepsilon)\ ;\ \varepsilon^R \text{ and } \mathcal{L}_1(\varepsilon^R) \text{ are constant and } \mathcal{L}_2(\Delta\varepsilon) \neq 0 \qquad (6)$$

We propose in this framework an original law for $\mathcal{L}_2(\Delta\varepsilon)$:

$$\mathcal{L}_2(\Delta\varepsilon) = \frac{\gamma.\mathcal{L}_1(\varepsilon^R)}{\tanh\left(\frac{\beta.\varepsilon^R}{f^*(\varepsilon^R)}\right)}.\tanh\left(\frac{\beta.\Delta\varepsilon}{f^*(\varepsilon^R)}\right) + \frac{(1-\gamma).\mathcal{L}_1(\varepsilon^R)}{\tanh\left(\frac{(1-\beta).\varepsilon^R}{f^*(\varepsilon^R)}\right)}.\tanh\left(\frac{(1-\beta).\Delta\varepsilon}{f^*(\varepsilon^R)}\right) \qquad (7)$$

Where β and γ are two material parameters which evolve between 0 and 1 and $f^*(\varepsilon^R)$ is a function of reference strain ε^R, previously defined in Dib et al. [28] in their Eq. 35.

This function is expressed such as:

$$\frac{1}{f^*(\varepsilon^R)} = A.\frac{\varepsilon^R}{\mathcal{L}_1(\varepsilon^R)}.\frac{d\mathcal{L}_1}{d\varepsilon}(\varepsilon^R) \qquad (8)$$

Where A is a non-unit parameter.

This modelling for $\mathcal{L}_2(\Delta\varepsilon)$ requires three parameters that have to be identified (A, β and γ). Considering the behaviour during first loading and during the loading/unloading process, the irreversible time independent stress $\sigma_{ti}(\varepsilon)$, requires the identification of five parameters (G, H, A, β and γ). Figure 3 (a), (b) and (c) gives respectively the influence of parameters β, γ and A, on the shape of the unloading/reloading curve. Figure 3 illustrates the shape of the irreversible time independent stress $\sigma_{ti}(\varepsilon)$, defined by the relations from (2) to (8), during a first load 0-a and a-b, and also during an unloading/reloading sequence a-0-a. According to definition (7) of law $\mathcal{L}_2(\Delta\varepsilon)$, which defines the cycle behaviour, Figure 3 shows that, when strain $\varepsilon = 0$, the cycle stress and its tangent modulus are null ($\sigma_{ti}(0) = 0$, horizontal asymptote). On these three figures, we adopt the same first load, characterized by relation (5) and by parameters $G = 50\,MPa$ and $H = 200\,MPa$. Likewise, the dashed curve for the unloading/reloading sequence is the same in the three figures and is defined by relations (5) to (8) with $A = 20$, $\alpha = \beta = 0{,}01$.

Taking into account relations (6) and (7), the derivative $\frac{d\mathcal{L}_2}{d\varepsilon}(\Delta\varepsilon)$ at the inversion point such as $\Delta\varepsilon = 0$, denoted $\frac{d\mathcal{L}_2}{d\varepsilon}(\Delta\varepsilon = 0)$ corresponds to the tangent modulus of $\sigma_{ti}(\varepsilon)$ at the inversion point, at the beginning of the unloading curve, and is expressed by:

$$\frac{d\mathcal{L}_2}{d\varepsilon}(\Delta\varepsilon = 0) = \mathcal{L}_1(\varepsilon^R).\left\{\frac{\gamma.\beta}{\tanh\left(\frac{\beta.\varepsilon^R}{f^*(\varepsilon^R)}\right)} + \frac{(1-\gamma).(1-\beta)}{\tanh\left(\frac{(1-\beta).\varepsilon^R}{f^*(\varepsilon^R)}\right)}\right\}.\frac{1}{f^*(\varepsilon^R)} \qquad (9)$$

Function $f^*(\varepsilon^R)$ takes into account the fact that the tangent modulus at the inversion point evolves as a function of the reference strain ε^R, the value of strain at inversion point (8). Indeed, (8) and (9) define an increasing monotonous evolution of the tangent modulus at inversion point $\frac{d\mathcal{L}_2}{d\varepsilon}(\Delta\varepsilon = 0)$, as a function of the ratio between the modulus just before the

inversion point $\frac{d\mathcal{L}_1}{d\varepsilon}(\varepsilon^R)$ and the sequent modulus $\frac{\mathcal{L}_1(\varepsilon^R)}{\varepsilon^R}$. This aspect is indicated by Figure 4 at inversion points A, B, C, D and E and on the evolution curve of modulus $\frac{d\mathcal{L}_2}{d\varepsilon}(\Delta\varepsilon = 0)$.

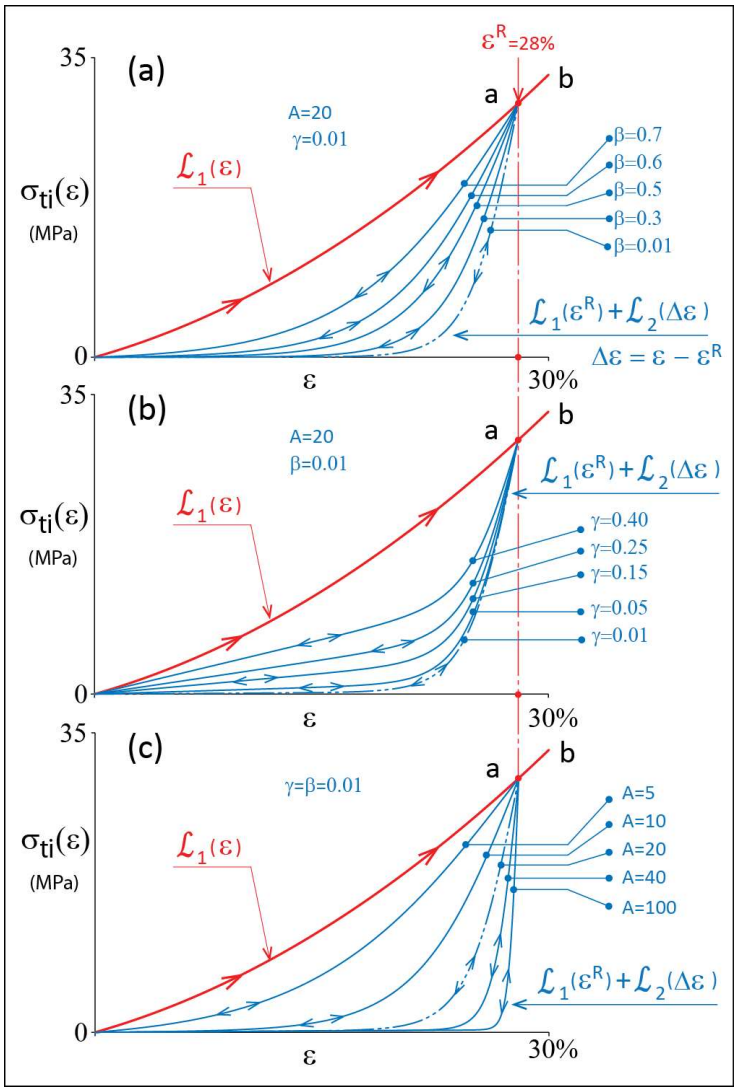

Figure 3: Influence of parameters β (a), γ (b) and A (c) on the unloading curve shape when strain at the load-inversion point is $\varepsilon^R = 28\ \%$ and the parameters of the first loading curve are maintained at the same value $G = 50\ MPa$ and $H = 200\ MPa$. The dashed curve is a common curve to the three figures (a), (b), (c) such as the parameters values are A =20, $\beta = \gamma = 0{,}01$.

Figure 4 illustrates the behaviour of the irreversible time independent stress $\sigma_{ti}(\varepsilon)$ with five unloading/reloading cycles: A0A, B0B, C0C, D0D and E0E. This figure describes the evolution of the modulus at the right of the inversion point $\frac{d\mathcal{L}_2}{d\varepsilon}(\Delta\varepsilon = 0)$, as a function of strain ε. This evolution is a monotonic increasing function, which is characterized by relations (8) and (9).

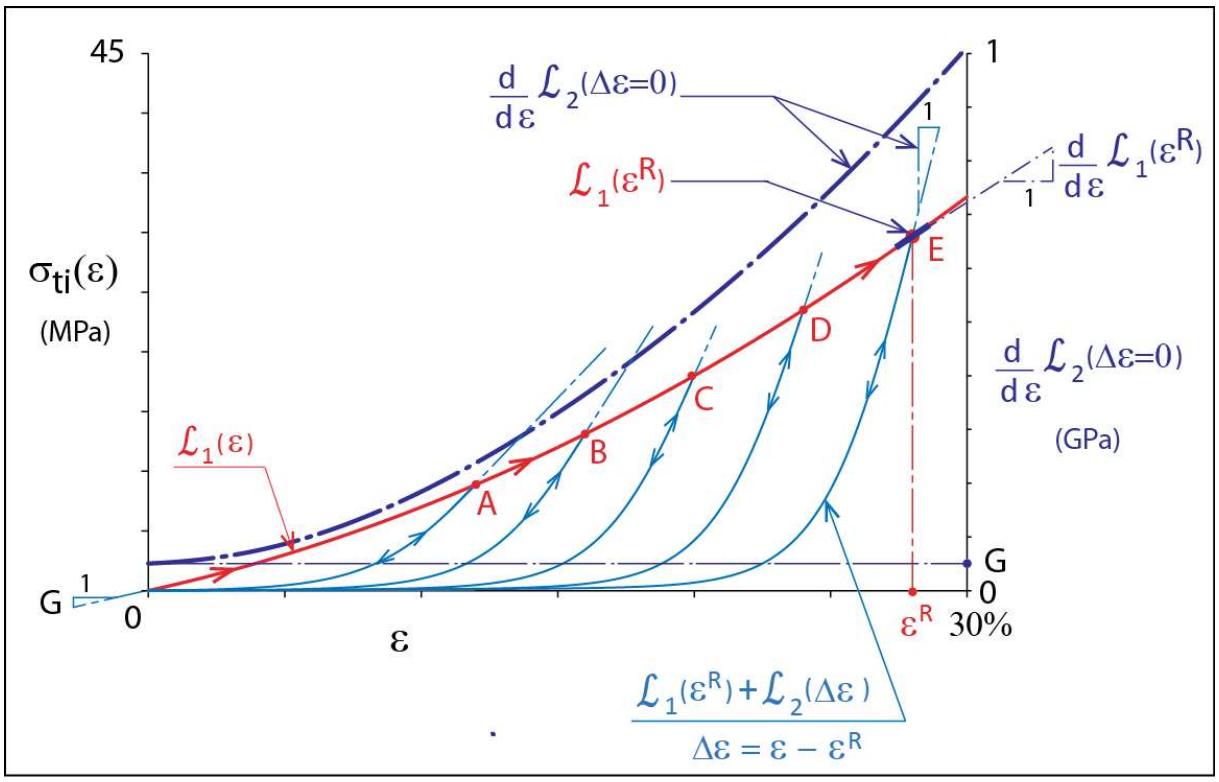

Figure 4: Illustration of the irreversible time independent stress $\sigma_{ti}(\varepsilon)$ during the first load and during the unloading/reloading processes with the inversion point ε^R (0.12 to 0.28 by step of 0.04 stood for by the points A, B, C, D and E). The parameters of the unloading curve are $\gamma = \beta = 0.01$ and $A = 20$ and the parameters of the first load are $G = 50\ MPa$ and $H = 200\ MPa$. A second curve in dashed line is given to show the evolution of modulus $\frac{d\mathcal{L}_2}{d\varepsilon}(\Delta\varepsilon = 0)$ as a function of strain. This evolution is also illustrated on the inversion points A, B, C, D and E on the curve of $\sigma_{ti}(\varepsilon)$.

Note that the formula $\frac{d\mathcal{L}_2}{d\varepsilon}(\Delta\varepsilon = 0)$ defined by relation (9) tends towards G when the strain tends towards zero (the value of G is indicated on the right axis of Figure 4). This leads to a quasi-elastic behaviour with a modulus that equals to G, to the right of the origin, taking into account definition (5) of the first load $\mathcal{L}_1(\varepsilon^R)$.

b) Viscous contribution

The visco-elastic stress $\sigma_v(\dot{\varepsilon})$ is described by a Maxwell-like rheological model with a variable viscosity $\eta(\dot{\varepsilon})$ depending on strain rate $\dot{\varepsilon}$, and appears under the form of a scalar differential equation (Dib et al. [28]):

$$\frac{\overset{\circ}{\sigma_v}}{K} + \frac{\sigma_v}{\eta(\dot{\varepsilon})} = \dot{\varepsilon} \qquad (10)$$

where, $\overset{\circ}{\sigma_v}(\dot{\varepsilon})$ stands for the viscous stress rate and K denotes a constant elastic modulus of the viscous contribution (in Figure 2). The viscosity evolution $\eta(\dot{\varepsilon})$ follows a five parameters Carreau-Yasuda model. [36] This model puts forward three main regimes: in the case of a weak strain rate, a Newtonian plateau where the viscosity is considered as constant and equals to η_0, and for higher values of the strain rate, a linear regime that corresponds to a Ostwald and De Waele power law. [37] The third regime corresponds to the case where $\dot{\varepsilon}$ tends to the infinite, then the viscosity tends to a limit value denoted η_∞. The viscosity $\eta(\dot{\varepsilon})$ can be finally expressed by:

$$\frac{\eta(\dot{\varepsilon})-\eta_\infty}{\eta_0-\eta_\infty} = \{1 + (\lambda.|\dot{\varepsilon}|)^a\}^{\frac{n-1}{a}} \qquad (11)$$

where, η_0 denotes the Newtonian plateau constant viscosity, η_∞ stands for the viscosity value for an infinite strain rate; λ and n are the parameters that define respectively the threshold and

the slope of the Ostwald and De Waele power law ; a is a parameter that models the transition between the constant and the linear parts of the behaviour.

Therefore, the definition of the viscous part $\sigma_v(\dot{\varepsilon})$ of the stress needs six parameters (K, η_0, η_∞, λ, n, a). By taking into account the irreversible time independent behaviour represented by $\sigma_{ti}(\varepsilon)$, the whole model for the global stress $\sigma(\varepsilon, \dot{\varepsilon})$ depends on eleven parameters that will be identified in the next part.

IV) Parameter-law identification

1) Identification of the irreversible time independent contribution during first load

Figure 5 illustrates the identification of the irreversible time independent behaviour during the first loading, defined by relations (3) and (5). This figure gives the comparison between $\mathcal{L}_1(\varepsilon^R)$, whose identified parameter values are in Table 1, and the time independent stress $\sigma_{ti}(\varepsilon\,, \zeta = 0)$ in the previous works of Bles et al. [9], obtained by fitting multiple experimental results of the stress at the ends of relaxation and creep stages for the straps of group A. In the paper of Bles et al. [9], $\sigma_{ti}(\varepsilon\,, \zeta = 0)$ is defined by relation (16), its evolution is illustrated by figure (26) and the values of the parameters for the straps of group A are given in Table 1.

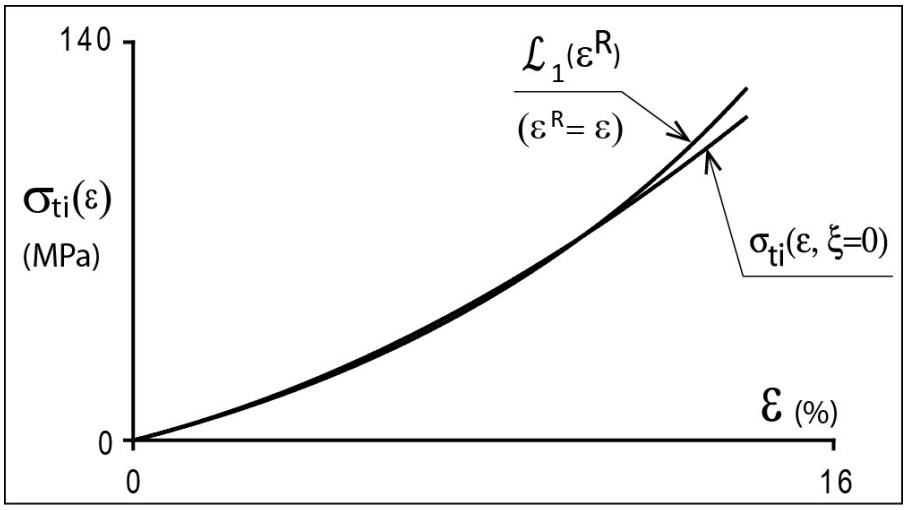

Figure 5: Comparison between $\sigma_{ti}(\varepsilon)$ once the parameters G and H are identified and the time independent stress $\sigma_{ti}(\varepsilon\,;\zeta = 0)$ obtained by fitting multiple experimental results of the stress at the ends of relaxation and creep stages for the straps of group A (Bles et al. [9]).

2) Identification of the irreversible time independent contribution during loading/unloading sequences

In order to identify the parameters present in the non-linear elastic contribution $\mathcal{L}_2(\Delta\varepsilon)$ defined by relation (7), we used the experimental data of stress obtained at the end of creep and relaxation periods during cycles. These experimental results were obtained by Bles et al. [9] during tests A36, A38 and are presented respectively in Figures 29 to 31 of their paper. Figure 6 gives the comparison of the irreversible time independent contribution identified and the experimental results. The values for the identified parameters A, β and γ involved in (7) and (8) appear in Table 1.

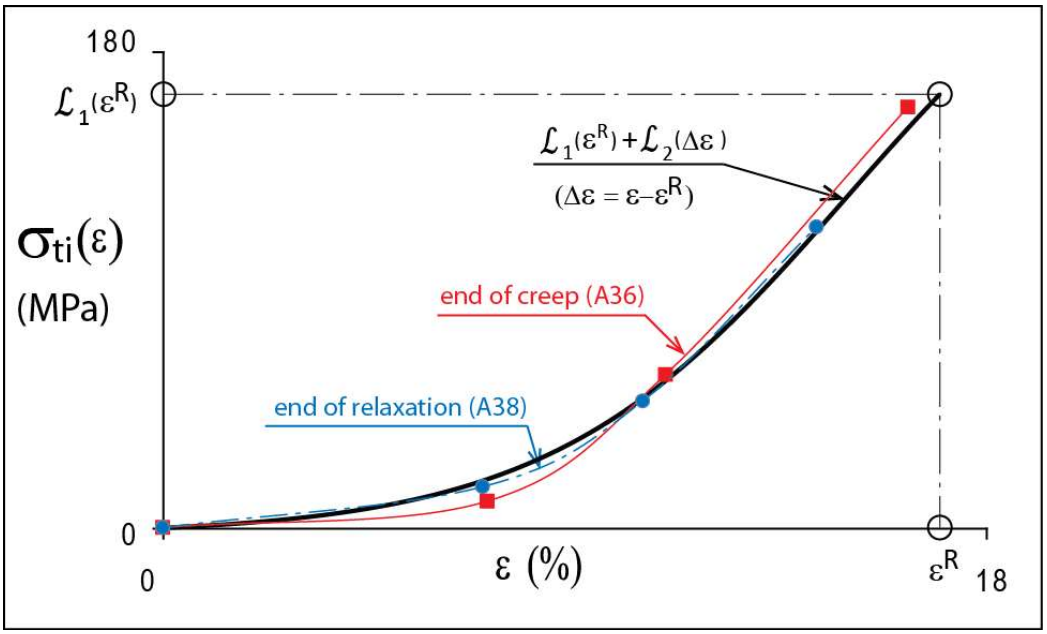

Figure 6: Diagram showing the stress state at the end of relaxation (A38) and creep (A36) tests (circle and square points respectively) and the fitting of the irreversible time-independent stress $\sigma_{ti}(\varepsilon)$ once the parameters A, β and γ are identified (thick line).

3) Identification of the viscous contribution

The viscous threshold in monotonous-loading tensile tests at a constant strain rate, characterized experimentally by Bles et al. [9], can be expressed by the following form:

$$\sigma_V{}^{\infty}(\varepsilon,\dot{\varepsilon}) = b^{\infty}(\varepsilon).log\left(\frac{\dot{\varepsilon}}{\dot{\varepsilon}_0}+1\right) \quad \text{and} \quad b^{\infty}(\varepsilon) = b_0.\left[\left(\frac{\varepsilon}{\varepsilon_b}\right)^3+1\right] \qquad (12)$$

Where, $\dot{\varepsilon}_0 = 10^{-\frac{\sigma_1}{b_0}}$ and $\sigma_1 = 34.21\ MPa$, $\varepsilon_b = 20\%$, $b_0 = 4.6\ MPa/decade$ are constants for the straps of group A. Relation (12) can be obtained by combining Eq. 7 and 8 of Bles et al. [9] This relation shows that the viscous threshold depends both on the strain, through the $b^{\infty}(\varepsilon)$ term, and on the strain rate. In the modeling framework adopted here, the viscosity only depends on the strain rate ((10) and (11)). Therefore, we adopt an approximate expression for the viscous threshold, characterized experimentally by neglecting the

dependence on strain. For that, the $b^{\infty}(\varepsilon)$ function is approximated by a constant mean value denoted b^{∞}, between b^{∞} (0) and b^{∞} (15%), such as:

$$b^{\infty} = 5.6\ MPa/decade \qquad (13)$$

Consequently, the expression of the viscosity of the strap, characterized experimentally, is written:

$$\eta(\dot{\varepsilon}) = \frac{\sigma_V{}^{\infty}(\dot{\varepsilon})}{\dot{\varepsilon}} = \frac{b^{\infty}.log\left(\frac{\dot{\varepsilon}}{\dot{\varepsilon}_0}+1\right)}{\dot{\varepsilon}} \qquad (14)$$

In Figure 7, this expression is illustrated by the experimental points placed in the experimental zone scanned by the authors between $\dot{\varepsilon} = 3.10^{-1}s^{-1}$ and $\dot{\varepsilon} = 10^{-5}s^{-1}s$. Figure 7 also illustrates the identification of the Carreau-Yasuda model whose parameter values are given in Table 1.

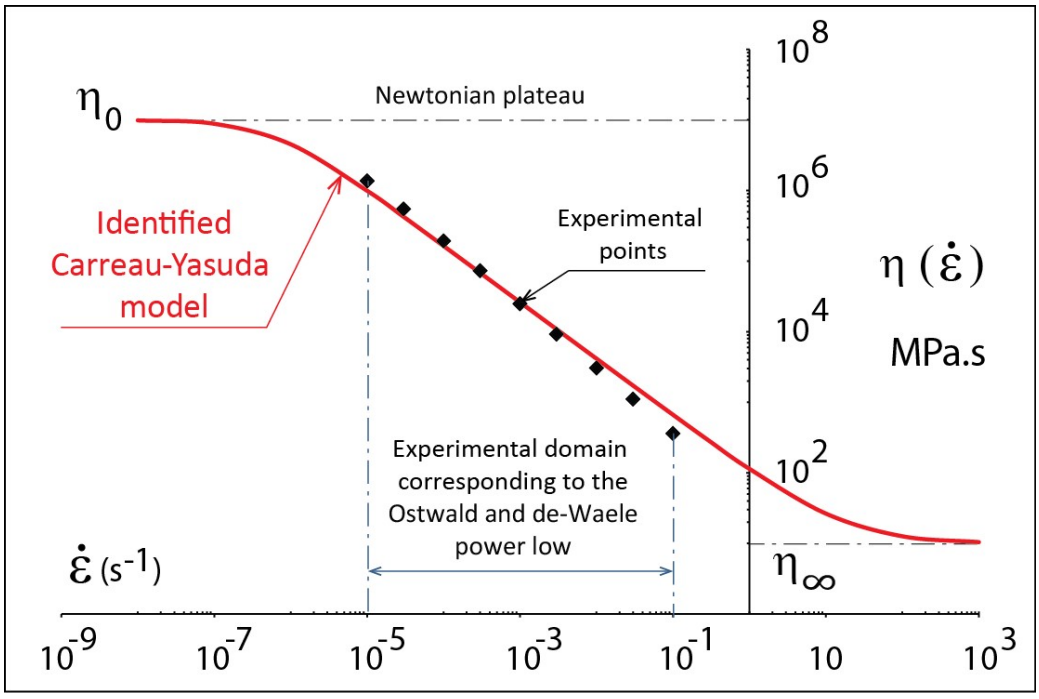

Figure 7. Identification of Carreau-Yasuda model by using the experimental data obtained by Bles et al. [9]

In Bles et al. [9], the elasticity modulus $E_V(\varepsilon)$ of the Maxwell-like viscoelastic model exhibits a nonlinear evolution as a function of the strain. This evolution is characterized by Figure 35 of the authors. In the context of the present study, a constant value is adopted for this modulus, denoted by K (Figure 2). This value corresponds to an average located between the beginning and the end of the evolution E_V in Figure 35 of the authors, such as:

$$K = 3{,}5\ GPa \qquad (15)$$

Stress contribution	Parameter	Value	Unit
$\sigma_{ti}(\varepsilon)$	G	391	MPa
	H	3	GPa
	A	10	-
	β	0,12	-
	γ	0,14	-
$\sigma_V(\dot{\varepsilon})$	η_∞	10	MPa/s
	η_0	10^7	MPa/s
	λ	$1{,}7.10^7$	s
	a	1	-
	n	0,2	-
	K	3,5	GPa

Table 1: Identified parameter values.

V) Exploitation of the constitutive model

1) Monotonous and cyclic tensile tests with different strain rates

Figure 8a shows the response of the model for the total stress $\sigma(\varepsilon, \dot{\varepsilon})$ in the case of monotonous tensile tests with different strain rates $\dot{\varepsilon}$ (from 10^{-5} s^{-1} to 10^{-1} s^{-1}). We obtain a behaviour close to the experimental observations in the case of monotonous tensile tests at different constant strain rates, for samples of group A performed in the works of Bles et al. [9] (Figure 8b).

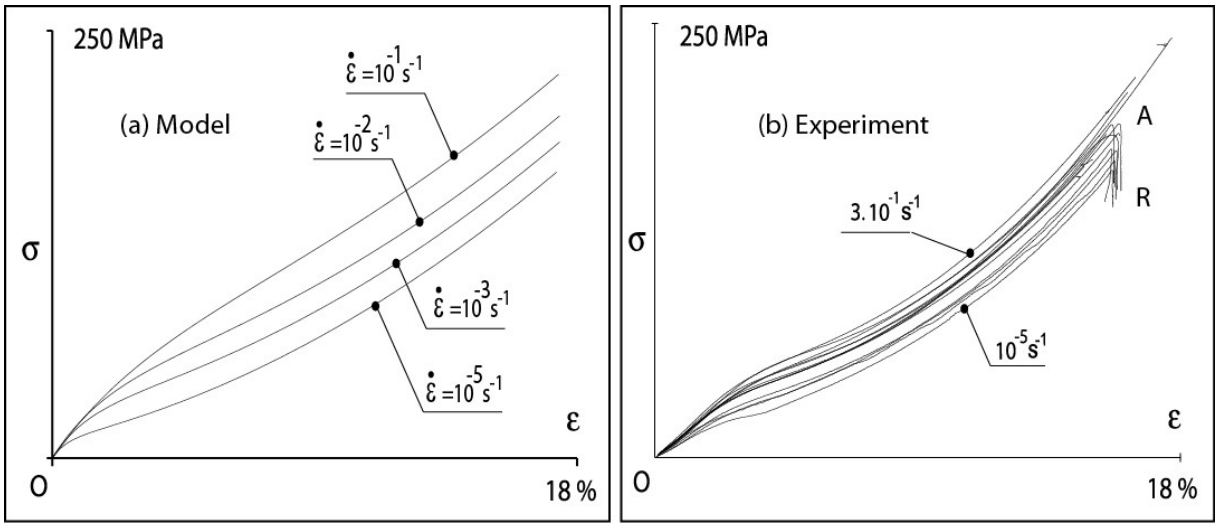

Figure 8: Comparison between model (a) and experiment (b) in the case of monotonous tensile tests, for strap samples of group A with different strain rates (from 10^{-5} s^{-1} to 10^{-1} s^{-1}); some experimental results (b) were ended by a relaxation sequence *AR*, at a constant strain.

Figure 9 shows on the same graph, the total stress $\sigma(\varepsilon, \dot{\varepsilon})$ and the irreversible time independent stress $\sigma_{ti}(\varepsilon)$ given by the model in the case of cyclic tensile tests (0abcdefg) with different strain rates $\dot{\varepsilon}$ (from 10^{-4} s^{-1} to 10^{-2} s^{-1}). During these cyclic tests, the absolute value of the strain rate remained constant and its sign changed at the reversal of the cycles. At the inversion points a, c and e, the stress-strain loops were limited by a given value of strain, and at the inversion points b, d and f by a stress value equal to zero. The result shows that the model is able to predict the typical bean shape of the stress-strain loops. This particular bean

shape is relatively pronounced in Figure 9a, for a relatively low strain rate ($\dot{\varepsilon} = 10^{-4}$ s^{-1}). This aspect of the behaviour of the model is qualitatively confirmed by all the experimental results of Bles et al. [9] and particularly by those of the C35 test on the straps of the group C (Figure 9 of Bles et al. [9]). Let us note that the stress-strain cycles shape is very sensitive to viscosity effects and to the shape of σ_{ti}.

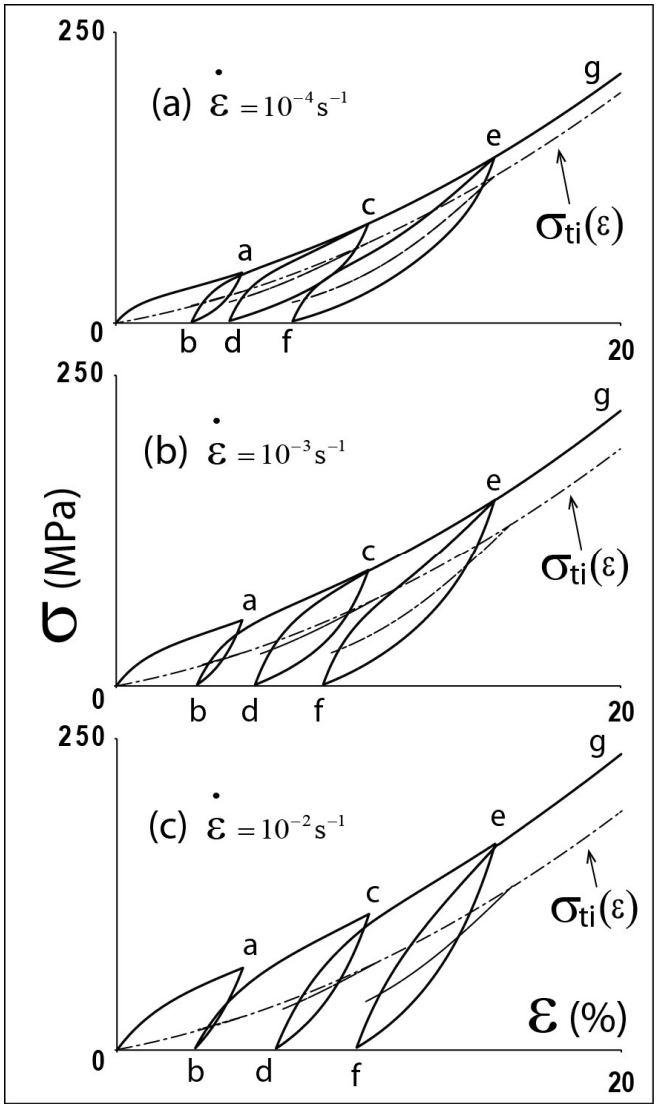

Figure 9: Response of the model for total stress in the case of cyclic tensile tests 0abcdefg with different strain rates; (a) 10^{-4} s^{-1}, (b) 10^{-3} s^{-1} and (c) 10^{-2} s^{-1}.

2) Mean stress relaxation during repeated cycles

During a loading made up of a monotonous loading followed by a series of repeated cycles between two fixed strains, the mean stress per cycle decreases with the number of cycles. There is a link between this phenomenon and the one of the time evolution of the stress during a relaxation stage. Figure 10 illustrates this behaviour.

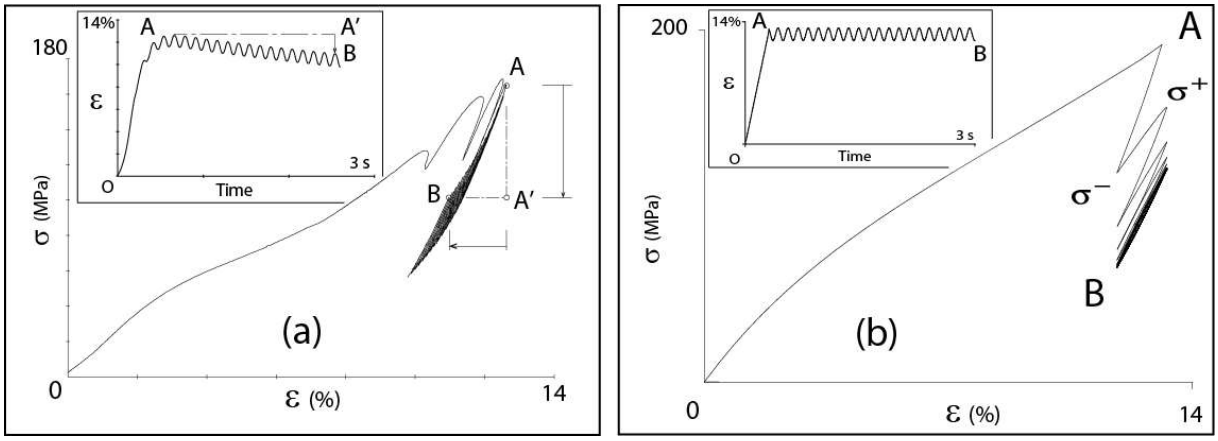

Figure 10: Qualitative comparison model-experiment during repeated cycles between two given strains: (a) Not published experimental result on a strap of group C in stress-strain diagram and the corresponding loading program in a strain-time diagram; (b) Modelling behaviour of a group-A strap, under the same type of loading; the loading program, with a duration of 3s, is composed of a monotonous tensile test *0A* followed by a sinusoidal loading *AB* at a frequency of 7.6Hz.

Figure 10 gives a qualitative comparison between an experimental result on a group-C strap (Figure 10-a) and a modelling result obtained with the parameters identified in Table 1, for the group-A strap (Figure 10-b). The loading program, shown in Figures 10-a and 10-b, consists typically of a monotonic tensile test 0A followed by a sinusoidal loading AB at a frequency of 7.6Hz. In the stress-strain diagram, the model response shows a crawling closed cycle (σ^+, σ^-), so that the mean stress per cycle decreases with the number of cycles. This phenomenon is confirmed by the experimental result of Figure 10-a. Let us note however, that

the program of loading of the experimental result presents a slight drift in strain A'B, during the phase of sinusoidal loading. Indeed the amplitude and the frequency of the cycle are constant, but the mean value of deformation exhibits a linear drift as a function of time between A and B. In the stress-strain diagram of Figure 10-a, we have indeed a closed cycle creeping vertically from point A to point A', so that the mean stress per cycle decreases with the number of cycles. However, there is also a horizontal sliding of the cycle, from point A' to point B, given the drift A'B of the strain in the loading program.

In order to understand the phenomenon of mean stress relaxation during repeated cycles, let us consider the loading OAB in Figure 11, composed of a first load OA and a series of cycles AB. Let us split this strain loading into a monotonous loading followed by a relaxation (loading OAR in Figure 11) and a symmetric cyclic loading between two fixed opposite strains (loading CB in Figure 11) ; so the time evolution of strain is the sum of the one of relaxation loading OAR and the one of symmetric cyclic loading CB.

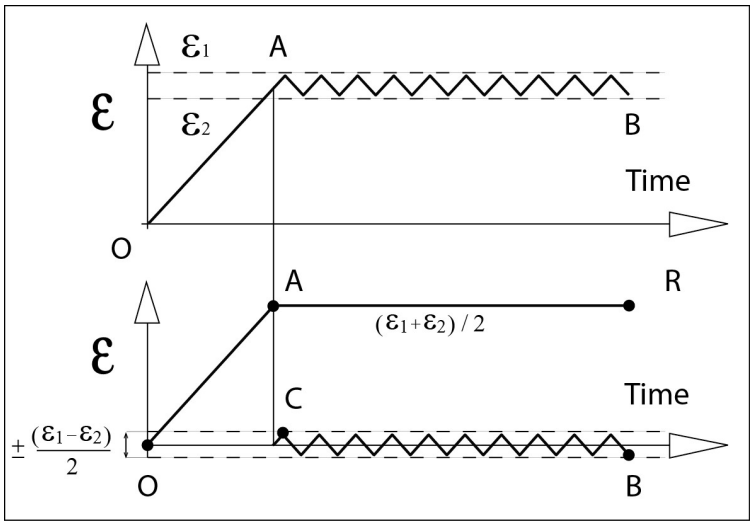

Figure 11: Splitting of strain loading OAB, into a monotonous loading followed by a relaxation (loading OAR) and a symmetric cyclic loading (loading CB).

The behaviour observed in Figure 10 seems to be linked to the Boltzmann's superposition principle: the stress response to the sum of two strain loading cases, of Figure 11, is then the sum of the two stress corresponding responses OAR and CB given on Figure.12-a. Figure 12-b gives, on one hand, the time evolution of the resulting superimposition of these two responses; on the other hand, this figure gives the time evolutions of σ+ and σ−, the stresses at the inversion points, which result of vertical translation of the temporal evolution of stress during the relaxation sequence. As a result, the evolution of mean stress, during cyclic loading CB, is merged with the evolution of stress during relaxation.

For this reason, the mean stress relaxation during repeated cycles is very close to the time evolution of the stress during the similar relaxation stage, as Figures 12b illustrates it.

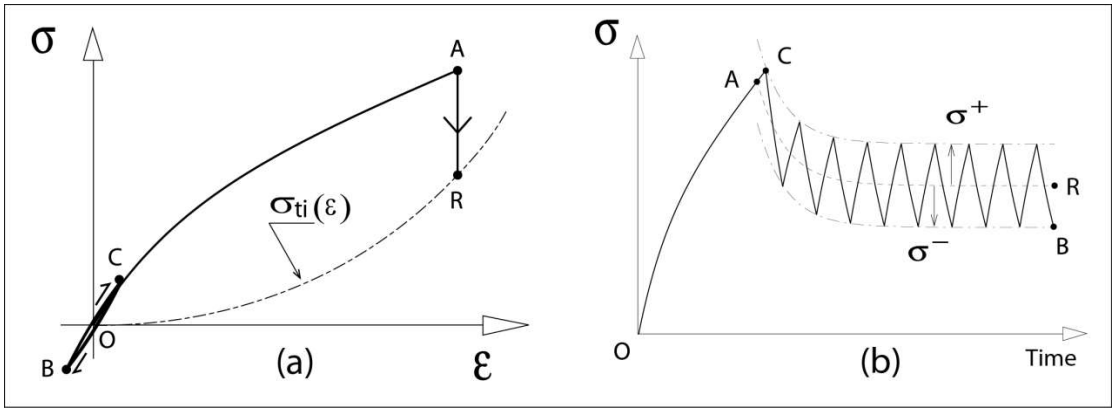

Figure 12: Superimposition of two responses to two loading sequences, in order to analyse the behaviour observed on Figure 10: (a) stress-strain responses to relaxation loading OAR and to symmetric cyclic loading CB, respectively; (b) time evolution of the superimposition of the two responses in stress to the two loading sequences OAR and CB; The two extreme dotted lines correspond to the temporal evolution AR translated vertically to reveal σ+ and σ−, that are the stresses at the inversion points.

Figure 13 gives more details about the modelling given by Figure 10b of repeated cycles between two given strains. On the stress-strain diagram of Figure 13-a, we superimpose the total stress and time independent stress. Figure 13-b gives the evolution of total stress as a function of time. The stress-strain cycle exhibits an important mean stress relaxation and finally evolves towards a stabilized cycle. When the strain amplitude is low and the strain rate is relatively high, the stabilized cycle tends towards an instantaneous elastic behaviour characterized by a modulus $K^{ins}(\varepsilon)$ defined such as:

$$K^{ins}(\varepsilon) = K + \frac{d\sigma_{ti}}{d\varepsilon}(\varepsilon) \qquad (11)$$

For weaker frequency values (less than 1 Hz), the cycle presents a quite open hysteresis loop. For higher frequencies, loops are rather closed. This can be explained by the fact that for high frequencies, the behaviour is mainly characterized by the instantaneous elasticity, whereas for lower frequencies, the visco-elastic behaviour is preponderant with a more and more active role of the damping. The mean stress or cycle relaxation observed on Figure 13-a is a viscous phenomenon. Indeed, the cycle gradually tends to centre around the σ_{ti} threshold.

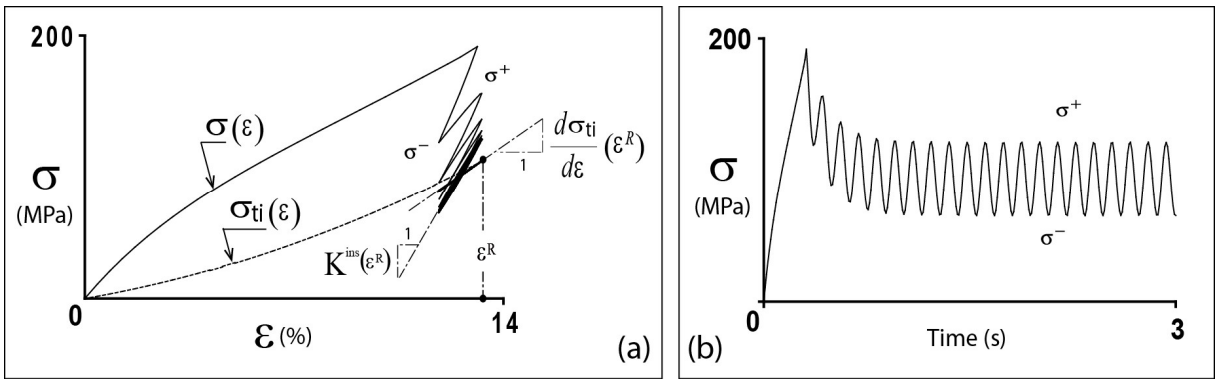

Figure 13: Modelling of the behaviour of a strap sample of group A during the repeated cycles between two given strains, presented in Figure 10-b and illustrated by Figure 12-b: (a)

stress-strain diagram with total stress and time independent stress; (b) total stress as a function of time.

Therefore, we can conclude that, in this loading case and to a certain extent, the nylon strap behaviour follows the Boltzmann's superposition principle, even though its visco-elasto-plastic behaviour is irreversible and nonlinear. This behaviour is well reproduced by the proposed model. This property is confirmed by the experimental results shown in Figure 14. Figures 14-a gives a not published experimental result, on a strap of group A, which corresponds to monotonous loading followed by a series of repeated cycles between two fixed strains, at constant strain rates (test A08). Test A07 is a monotonic OA test at constant strain rate ($\dot{\varepsilon} = 10^{-2}$ s^{-1}), which ends with an AR relaxation. The result of this test is a part of the results presented in Figure 8 and it is represented by the evolution as a function of time of the OAR stress in Figure 14-b. In this figure, we also give the evolution of stress as a function of time OAB of the cyclic test A08. This figure makes it possible to compare qualitatively the time evolution of the average stress of the AB cycle with the time evolution of the stress during relaxation. Figures 14-c and 14-d give more precise comparisons of stress evolution at right and left inversion (test A08) and stress during the relaxation sequence (test A07). Figures 14-c and 14-d show that mean stress evolution, during cyclic loading, is very close to the evolution of stress during relaxation. This result confirms that, in this loading case, the nylon strap behaviour follows the Boltzmann's superposition principle.

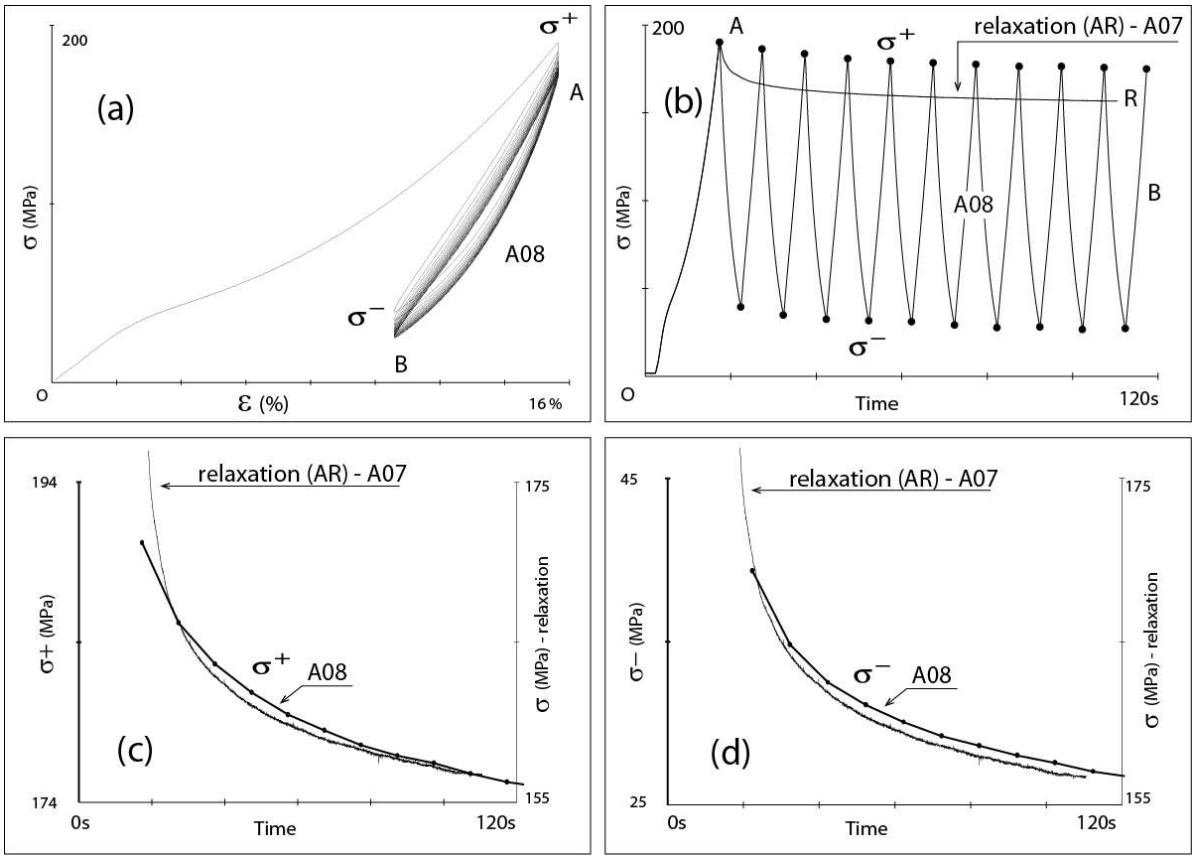

Figure 14: Comparison of stress evolution during relaxation AR (test A07) and at inversion points (σ+, σ–) of repeated cycles between two given strains (test A08), at constant strain rate ($\dot{\varepsilon} = 10^{-2}$ s^{-1}): (a) not published experimental result, on a strap of group A; monotonous loading followed by a series of repeated cycles between two fixed strains (test A08); (b) time evolution of stress during tests A07 and A08; (c) comparison between the time evolutions of stress at right inversion (test A08) and during relaxation (test A07); (d) comparison between the time evolutions of stress at left inversion (test A08) and during relaxation (test A07).

3) Cyclic tensile tests with creep and relaxation sequences

Figure 15 gives a model-experiment comparison of test A38. This test corresponds to a cyclic tensile loading interrupted by relaxation periods, of one-hour duration, during which the strain is constant. Test A38 presents one loading–unloading cycle *0gngs*. The absolute value of strain rate is maintained constant during the loading and unloading processes, at a value of $10^{-3}s^{-1}$. During the relaxation periods, the stress may decrease or increase according to the location of the relaxation sequence in loading–unloading process. Thus, for example, if we consider the relaxation sequence *hi* during the unloading sequence *gn*, the stress decreases, but on the other hand, during the relaxation sequences *jk* and *lm*, the stress increases. This result shows that the model forecasts the correct shape of stress-strain hysteresis loop and predicts perfectly the direction of stress evolution during relaxation periods, whatever their position in the first loading or in loading/unloading process.

Figure 16 gives a model-experiment comparison of test A36. This test corresponds to a cyclic tensile loading interrupted by creep periods, of one-hour duration, during which the stress is constant. Test A36 presents one loading–unloading cycle *0eleq* and finished with a creep sequence *qr*. The absolute value of stress rate is maintained constant during the loading and unloading processes, at a value of $32.9\ MPa/s$. Similarly to the case of relaxation sequences, during the creep periods, strain may decrease or increase according to the location of the creep sequence in loading–unloading process. Indeed, during creeps *fg* and *hi*, for example, Figure 16 shows a change in the strain evolution direction. Taking into account the coupling between the viscous effects and the time-independent effects, the behaviour during the creep sequences is complex and non-intuitive. Indeed, we note that during the creep sequences *hi* and *jk*, the test sample shortens despite the tensile stress is positive. In the same way, during the creep sequence *mn*, the sample is shortened even though the stress is almost zero.

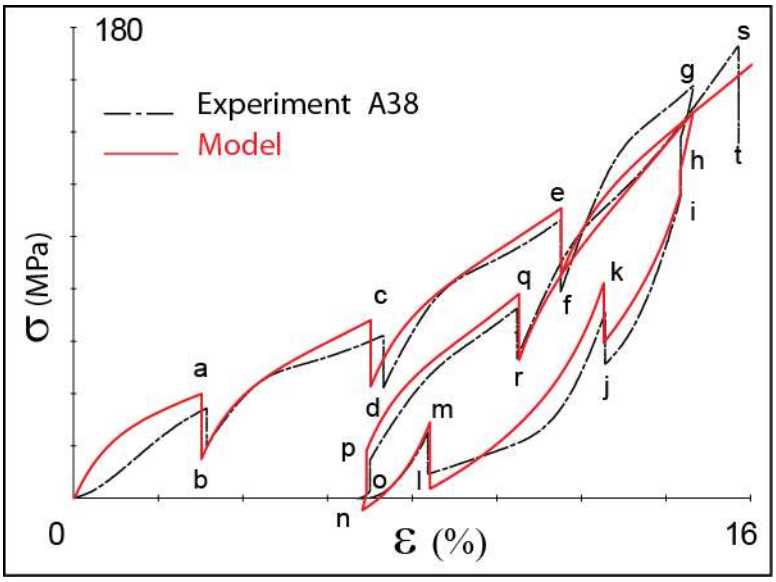

Figure 15: Model-Experiment comparison in cyclic loadings with relaxation sequences: $\dot{\varepsilon} = 10^{-3}$ s^{-1} and relaxation sequence with a duration of 1h (Test A38 in Bles et al. [9]).

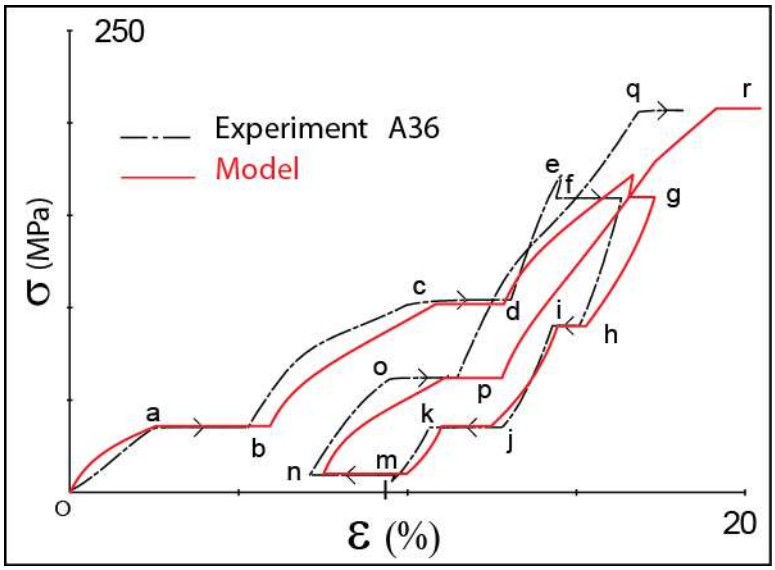

Figure 16: Model-Experiment comparison in cyclic loadings with creep sequences: $\dot{\sigma} = 32{,}9$ MPa.s^{-1} and creep sequence with a duration of 1h (Test A36 in Bles et al. [9]).

This result shows that the model forecasts the correct shape of stress-strain hysteresis loop and predicts perfectly the direction of the strain evolution during creep periods, whatever their position in the first loading or in loading/unloading process.

For the same test A36, Figure 17 gives the model – experiment comparison of time evolution of strain. This figure allows us to observe the shape of the time evolution of strain during creep periods for strap material. Once again, this result shows that the model forecasts the correct shape of time evolution of strain during creep periods, with a quite good precision.

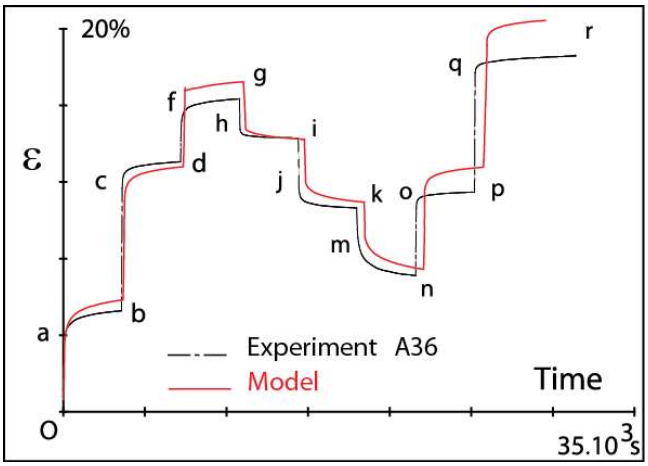

Figure 17: Model – experiment comparison; diagram strain versus time (test A36).

VI) Conclusion

An original one-dimensional model is proposed to describe the mechanical behaviour of woven materials, shaped in uniaxial form. This model is based on the superimposition of two stress contributions: a non-Newtonian visco-elastic stress and a time-independent stress. The non-Newtonian visco-elastic stress is described by a Maxwell-like rheological model, with a constant elastic modulus and a variable viscosity depending on strain rate. To describe the visco-elastic behaviour, we adopt the Carreau-Yasuda's model. The time-independent stress stands for a particular irreversible behaviour, linked to the loading history, which presents an irreversible non-linear behaviour during first loading and a non-linear elastic behaviour during unloading-reloading processes. This model neglects the thickness of the time independent hysteresis loops during the unloading-reloading processes while preserving the irreversible character of elastoplastic-type behaviour. The proposed model depends on eleven parameters;

which can be identified by monotonic tensile tests at different strain rates and cyclic tensile tests with relaxation and/or creep sequences.

The model was validated by comparing its predictions with a set of experimental results, carried out on polyamide 6-6 (PA66) woven straps.

Despite the simplifying assumptions adopted for its definition, the model presents relevant modelling results of strap behaviour. Indeed, the model provides a good description of the stress as function of the strain rate, in first load as well as in load/unload loops. During which, the stress-strain cycles shape is very sensitive to viscosity effects and to the shape of $\sigma_{ti}(\varepsilon)$. Furthermore, the model is able to predict the typical bean shape of stress-strain loops, generally observed in the behaviour of synthetic polymer ropes. In addition, it should be noted that the phenomenon of mean stress relaxation during repeated cycles, is well taken into account by the model.

Finally, we note that the model forecasts in a satisfactory manner the shape of stress-strain hysteresis loops and predicts perfectly the direction of strain or stress evolution during creep or relation periods, whatever their position in the first load or in loading/unloading process.

References

1. HORN GP and KURATH P. Failure of firefighter escape rope under dynamic loading and elevated temperatures. In : *Dynamic Behavior of Materials, Volume 1*, *proceeding of the 2010 annual conference of the society for experimental mechanics series on experimental and applied mechanics* (ed T. Proulx), 2011. p. 353-359. New York: Springer.

2. Spierings A and Stämpfli R. Methodology for the development of an energy absorber: application to worker security ropes. *Int J Impact Eng* 2006; 32: 1370–1383.

3. Del Vecchio CJM. *Lightweight materials for deep water moorings*, PhD Thesis, University of Reading, UK, 1992.

4. Banfield S. and Casey N. Evaluation of fibre rope properties for offshore mooring. *Ocean Eng 1988*; 25: 861–879.

5. Fernandes AC, Del Vecchio CJM and Castro GAV. Mechanical properties of polyester mooring cables. *Int. J. Offshore Polar Eng* 1999; 9:208–213.

6. Francois M and Davies P. Characterization of polyester mooring lines. IN: *ASME 27th international conference on offshore mechanics and artic engineering* (OMAE2008), Estoril, Portugal, 2008, vol. 1, pp.169–177,.

7. Chevillotte Y. *Characterization of the long-term mechanical behavior and the durability of polyamide mooring ropes for floating wind turbines*. PhD Thesis. Univ. Bretagne Loire, Engineering school ENSTA Bretagne, France, 2002.

8. Chevillotte Y, Marco Y, Bles G et al. Fatigue of improved polyamide mooring ropes for floating wind turbines. *Ocean Eng 2020*; 199:107011.

9. Bles G, Nowacki W and Tourabi A. Experimental study of the cyclic visco-elasto-plastic behaviour of a polyamide fibre strap. *Int. J. Solids Struct* 2009; 46: 2693–2705.

10. Bain C. *Compréhension et modélisation des mécanismes de contact des câbles en PE ultra haute densité*. PhD Thesis, Univ. de Bretagne Occidentale, école ENSTA Bretagne, France, 2020.

11. Bain C, Davies P, Bles G et al. Influence of bedding-in on the tensile performance of HMPE fiber ropes. *Ocean Eng* 2020; 203:107144.

12. ASTM D885-03: 2003. Standard test methods for tire cords, tire cord fabrics, and industrial filament yarns made from manufactured organic-base fibers. ASTM international, USA.

13. Demsar A, Bukosek V, and Kljun A. Dynamic mechanical analysis of nylon 66 cord yarns. *Fibres Tex East Eur* 2010; 18:29–33.

14. Ramazani S, Morshed M and Ghane M. Effect of service temperature on structure and mechanical properties of polyamide 6 & 66 tyre cords. *J Polym Res* 2011; 18:781–792.

15. Li X, Wei Y, Feng Q et al. Mechanical behavior of nylon 66 tyre cord under monotonic and cyclic extension: Experiments and constitutive modeling. *Fibers and Polym* 2017; 18:542–548.

16. Tian L, Wang D and Wei Q. Study on dynamic mechanical properties of a nylon-like polyester tire cord. *J. Eng. Fibers Fabr* 2019; 14:17.

17. Che J, Zhang Z, Hou J et al. Modeling of fibrous tow transmission considering residual strain and friction. *Tex Res J* Epub ahead of print February 15, 2021. DOI: 10.1177/0040517521993483.

18. Leech C. The modelling of friction in polymer fibre ropes. *Int. J. Mech. Sci* 2002; 44:621–643.

19. Leech C, Hearle J, Overington M, et al. Modelling tension and torque properties of fibre ropes and splices. In: *Proceedings of the third international offshore and polar engineering conference*, Singapore, 6 June-11 June 1993.

20. Beltran J and Williamson E. Degradation of rope properties under increasing monotonic load. *Ocean Eng* 2005; 32:826–844.

21. Ghoreishi S, Cartraud P, Davies P, et al. Analytical modeling of synthetic fiber ropes subjected to axial loads. part i: A new continuum model for multilayered fibrous structures. *Int. J. Solids Struct* 2007; 44:2924–2942.

22. Ghoreishi S, Davies P, Cartraud P, et al. Analytical modeling of synthetic fiber ropes. part ii: A linear elastic model for 1 + 6 fibrous structures. *Int. J. Solids Struct* 2007, 44:2943–2960.

23. Toomey C.J. *The dynamic behavior of nylon and polyester rope under simulated towing conditions.* Master's thesis, Massachusetts Institute of Technology, USA, 1988.

24. Davies P, Huard G, Grosjean F et al. Creep and relaxation of polyester mooring lines. In: *Proceedings of the offshore technology conference.* (OTC 12176), Houston, Texas, 1 May-4 May 2000.

25. Lechat C. *Comportement mécanique de fibres et d'assemblages de fibres en polyester pour cables d'amarrage de plates-formes offshore (mechanical behavior of polyester fibers and polyester- fiber assemblies for mooring ropes of offshore platforms)*. PhD Thesis. Ecole des Mines de Paris, France, 2007.

26. Pham H.D, Cartraud P, Schoefs F, et al. Dynamic modeling of nylon mooring lines for a floating wind turbine. *Appl Ocean Res* 2019; 87:1–8.

27. Bles G. *Bases thermomécaniques de la modélisation du comportement des matériaux tissés et des polymères solides (thermomechanical basis of the behavior modelization of woven materials and solid polymers)*. PhD Thesis. Univ. Joseph Fourier Grenoble 1, 2002, France.

28. Dib W, Bles G, Blaise A et al. Modelling of cyclic visco-elasto-plastic behaviour of coated woven fabrics under biaxial loading and finite strain. *Int. J. Solids Struct* 2018, 154:147–167.

29. Chailleux E and Davies P. Modelling the non-linear viscoelastic and viscoplastic behaviour of aramid fibre yarns. *Mech. Time-Depend. Mater* 2003; 7:2693–2705.

30. Davies P, Chailleux E, Bunsell A et al. Prediction of the long term behavior of synthetic mooring lines. In: Proceedings of the offshore technology conference. (OTC15379), Houston, Texas, 5 May-8 May 2003.

31. Chailleux E and Davies P. A non-linear viscoelastic viscoplastic model for behavior of polyester fibres. *Mech. Time-Depend. Mater* 2005; 9:147–160.

32. Huang W, Liu H, Lian Y et al. Modeling nonlinear creep and recovery behaviors of synthetic fiber ropes for deepwater moorings. *Appl Ocean Res* 2012; 39:113–120.

33. Flory J.F and Ahjem V. Testing polyester fiber rope for six change-in-length properties (6 cilp). In: *Conference MTS/IEEE Oceans*, Bergen, Norway, June 10-14, 2013.

34. Falkenberg E, Ahjem V, Larsen K, et al. Global performance of synthetic rope mooring systems - frequency domain analysis. In: *Proceedings of the ASME 30th international conference on ocean, offshore and arctic engineering*, Rotterdam, Netherlands, June 19-June 24 2011.

35. Falkenberg E, Yang L and Ahjem V. The syrope method for stiffness testing of polyester ropes. In: Proceedings of the ASME 37th international conference on ocean, offshore and arctic engineering, Madrid, Spain, June 17-June 22 2018, paper no. V001T01A067.

36. Yasuda, K. *Investigation of the analogies between viscometric and linear viscoelastic properties of polystyrene fluids*, PhD Thesis, Massachusetts Institute of Technology, Cambridge (Massachusetts), USA, 1979.

37. Bird RB, Armstrong RC and Hassager O. *Dynamics of polymeric liquids*, Vol. 1: Fluid mechanics, 1987.